The Astrophysical Journal Letters, 768:L2 (4pp), 2013 May 1 doi:10.1088/2041-8205/768/1/L2

PEAK FLUX DISTRIBUTIONS OF SOLAR RADIO TYPE-I BURSTS FROM HIGHLY RESOLVED SPECTRAL OBSERVATIONS

K. Iwai[1], S. Masuda[2], Y. Miyoshi[2], F. Tsuchiya[3], A. Morioka[3], and H. Misawa[3]
[1] Nobeyama Solar Radio Observatory, National Astronomical Observatory of Japan, Nobeyama, Nagano 384-1305, Japan; kazumasa.iwai@nao.ac.jp
[2] Solar-Terrestrial Environment Laboratory, Nagoya University, Nagoya, Aichi 464-8601, Japan
[3] Planetary Plasma and Atmospheric Research Center, Tohoku University, Sendai, Miyagi 980-8578, Japan
Received 2013 January 21; accepted 2013 March 28; published 2013 April 10

ABSTRACT

Solar radio type-I bursts were observed on 2011 January 26 by high resolution observations with the radio telescope AMATERAS in order to derive their peak flux distributions. We have developed a two-dimensional auto burst detection algorithm that can distinguish each type-I burst element from complex noise storm spectra that include numerous instances of radio frequency interference (RFI). This algorithm removes RFI from the observed radio spectra by applying a moving median filter along the frequency axis. Burst and continuum components are distinguished by a two-dimensional maximum and minimum search of the radio dynamic spectra. The analysis result shows that each type-I burst element has one peak flux without double counts or missed counts. The peak flux distribution of type-I bursts derived using this algorithm follows a power law with a spectral index between 4 and 5.

Key words: Sun: corona – Sun: radio radiation

1. INTRODUCTION

Type-I noise storms are one of the most frequently observed solar radio phenomena in the metric frequency range. They have two components: short-duration (0.1–1 s), narrowband ($\delta f = f \times$ several %) emission, called type-I bursts, and long-duration (hours to days), wideband ($\delta f \sim f$) continuum emission. The bursts and continuum emission are emitted simultaneously, and both are highly circularly polarized (up to 100%). The sense of polarization is the ordinary mode. Therefore, they are thought to be plasma emission at the local plasma frequency. Elgarøy (1977) summarized the observational results for type-I noise storms.

Several models have been proposed to explain type-I noise storms. Benz & Wentzel (1981) suggested that a newly emerging magnetic field could interact with a pre-existing coronal magnetic field, and reconnections could produce non-thermal electrons. These non-thermal electrons could generate Langmuir waves. Spicer et al. (1982) suggested that an emerging magnetic field may produce shocks, at which electrons may be accelerated. These accelerated electrons excite upper hybrid waves via a loss-cone instability. Nevertheless, the detailed generation processes of type-I noise storms have not been well understood.

The occurrence frequency distributions of a peak flux (or a total released energy) have been investigated in order to understand flares. The peak flux distribution of flares follows a power law in almost all observation bands, such as hard X-rays (Hannah et al. 2011), soft X-rays (Shimizu 1995), and microwaves (Akabane 1956). The peak flux distribution of flare sub-structures also follows a power law such as decimetric millisecond spikes with the spectral index of 2.99±0.63 and hard X-ray pulses with the spectral index of 1.46±0.34 (Aschwanden et al. 1998).

The peak flux distributions of low-frequency radio bursts are more complicated because there are several peak flux distributions that suggest different generation processes. For example, power-law distributions can be explained by the concept of self-organized criticality (SOC; Aschwanden 2011). Log-normal distributions of radio bursts can be explained by a stochastic growth theory (Cairns & Robinson 1998). The unstable velocity distribution of electron cyclotron maser emission can produce exponential distributions (Robinson et al. 1996).

The peak flux distribution of type-III bursts follows a power law with a spectral index of 1.45 ± 0.31 (Aschwanden et al. 1998). Interplanetary type-III storms or micro type-III bursts are observed in the decimetric to kilometric range. Their peak flux distributions follow a power law with a spectral index of 2.1 (Eastwood et al. 2010) or 3.6 (Morioka et al. 2007). Log-normal distributions have also been observed in interplanetary type-III storms (Cairns & Robinson 1998).

Metric and decimetric spikes are known to be radio bursts that have fine spectral structures. Power-law distributions with a spectral index smaller than 2 were observed by Nita et al. (2008) and by Meszarosova et al. (2000). However, exponential distributions were also reported by Robinson et al. (1996), Aschwanden et al. (1998), Meszarosova et al. (2000), and Rozhansky et al. (2008).

For type-I bursts, there are only a few observational results in which their peak flux distributions were investigated. Mercier & Trottet (1997) studied the peak flux distributions of type-I bursts at several fixed frequency bands using the Nancay Radio Heliograph. They suggested that type-I bursts follow a power-law distribution with a spectral index of about 3. Ramesh et al. (2013) studied the peak flux distributions of type-I bursts at 80 MHz using the Gauribidanur radioheliograph and polarimeter. They observed a power-law distribution of type-I bursts with a spectral index of 2.2–2.7.

The lack of observational results and detailed data analysis are important problems. Type-I noise storms have complex spectral structures that make burst detection difficult. In previous studies, bursts were usually detected in fixed frequency bands or limited frequency ranges owing to equipment limitations or numerous instances of radio frequency interference (RFI). In addition, the resolution of the radio spectra in some previous studies was limited in time and/or frequency, and Isliker & Benz (2001) suggested that measurements with insufficient

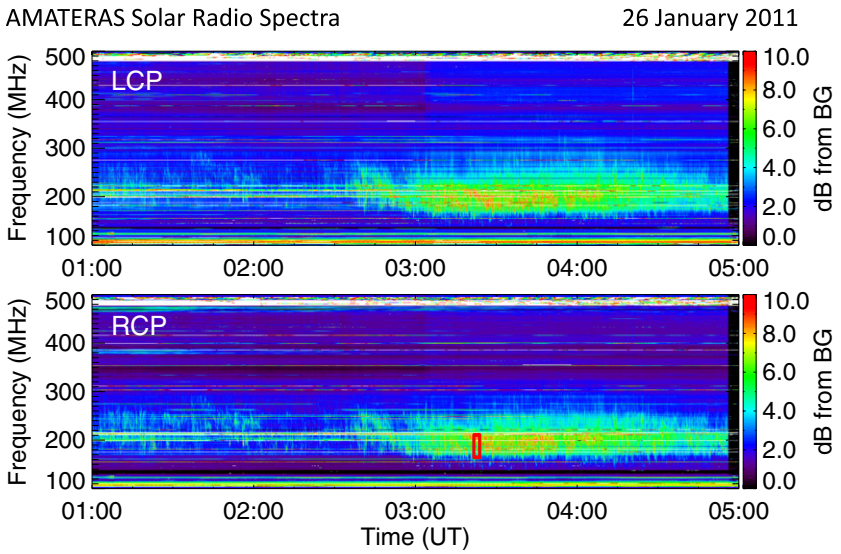

Figure 1. Radio dynamic spectra observed with AMATERAS on 2011 January 26. The top and bottom panels are LCP and RCP components, respectively. BG: background.

time and frequency resolution may cause unrealistic peak flux distribution.

We developed a two-dimensional auto burst detection algorithm that can remove RFI and distinguish an individual type-I burst element from complex type-I noise storm spectra. Then we derived the peak flux distributions of type-I bursts using AMATERAS (the Assembly of Metric-band Aperture TElescope and Real-time Analysis System; Iwai et al. 2012b), a solar radio telescope that can distinguish the fine spectral structures of metric radio bursts with high time and frequency resolution.

The instrument and data set used in this study are described in Section 2. The analysis methods that remove RFI and derive individual burst elements are given in Section 3. The observed peak flux distributions are summarized and discussed in Section 4.

2. OBSERVATIONS

AMATERAS is a solar radio telescope for spectropolarimetry in the metric range. It enables us to observe solar radio bursts at frequencies of 150–500 MHz with a 10 ms accumulation time and 61 kHz bandwidth. It is suitable for observing the characteristics of the fine spectral structures of solar radio bursts. Simultaneous observations of both the left-handed circularly polarized (LCP) component and the right-handed circularly polarized (RCP) component are possible. This antenna tracks the Sun every 30 s.

The type-I noise storms analyzed in this study were observed on 2011 January 26. Figure 1 shows radio dynamic spectra observed with AMATERAS on that day. Type-I emissions were observed mainly between 1:00 and 4:00 UT in the frequency range between 150 MHz (lower limit of the observation system) and 300 MHz. The flux densities of the RCP and LCP components are almost the same. Hence, the RCP component is shown in the following data analysis. Figure 2(a) shows a zoomed-in image of the part of the radio spectra indicated by a red rectangle in Figure 1. We can recognize many burst elements in the type-I noise storm spectra. The horizontal lines in the spectra are all RFI. Type-I bursts observed between 3:00 and 4:00 are used in the present data analysis. No C-class or larger flares or coronal mass ejections (CMEs) were reported during this period.[4,5] Hence, the type-I modulation by flares (Aurass et al. 1990, 1993) or CMEs (Chertok et al. 2001; Iwai et al. 2012a) can be neglected.

Figure 2(c) shows a zoomed-in image of the part of the radio spectra indicated by a white rectangle in Figure 2(b). Figure 2(d) shows a radio light curve of the burst element in Figure 2(c) at its peak flux band (179.5 MHz). The burst flux shows a smooth light curve without significant sub-structures. Hence, we define this structure as a fundamental burst element. Most of the observed fundamental burst elements have a typical duration of several hundred milliseconds and a typical bandwidth of several megahertz. Therefore, the following data analysis deals with radio bursts at these scales.

3. DATA ANALYSIS AND RESULTS

The spectral structures of type-I noise storms are complex and contain considerable RFI, as shown in Figure 2(a). In addition, a type-I noise storm has two components: the spiky type-I burst component and slowly varying continuum component. These two components are superposed on each other. To derive the peak flux distribution of the burst elements, we developed an analysis algorithm that can recognize the fundamental spectral structure of type-I bursts in complex noise storm spectra that contain considerable RFI.

In the AMATERAS system, the signal level of the quiet Sun is much higher than the background noise level at the observation site. That means that all of the RFI that contaminates the solar observations is artificial signals that have narrow emission bands at fixed frequencies, such as broadcasting signals. In contrast, a type-I burst has a broader emission bandwidth. A moving median filter along the frequency axis is effective for filtering out narrowband fixed-frequency signals (Kontogeorgos et al. 2006). We used a moving median filter with a bandwidth of 610 kHz (10 bins) along the frequency axis. Figure 2(b) shows the same radio spectra as Figure 2(a) after the moving filter's passage. Most of the RFI disappears from the noise storm spectra, while burst elements maintain their original shapes. This is because AMATERAS has a continuous observation band with a 61 kHz

[4] http://st4a.stelab.nagoya-u.ac.jp/hinode_flare/
[5] http://cdaw.gsfc.nasa.gov/CME_list/

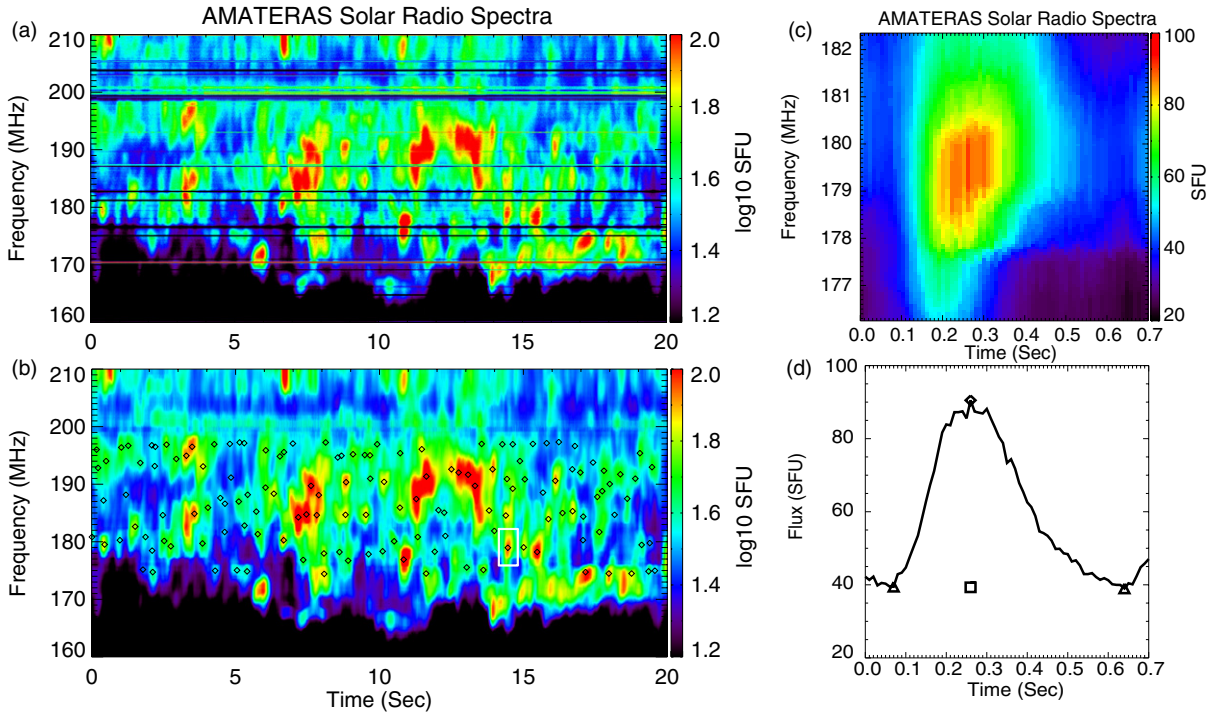

Figure 2. (a) Zoomed-in image of the part of the radio spectra indicated by red rectangle in Figure 1. (b) Same radio spectra as panel (a) after moving the filter's passage. The black diamonds are peaks of type-I bursts. (c) Zoomed-in image of the part of the radio spectra indicated by white rectangle in panel (b). (d) The radio light curve of the burst element in panel (c) at 179.5 MHz. The diamond indicates the burst peak, the triangles indicate background continuum, and the rectangle indicates the approximated background continuum flux at the peak time of the burst component.

bandwidth, which is significantly narrower than the typical bandwidth of type-I bursts. Hence, the radio spectra still have sufficient frequency resolution after the moving median filter's passage.

After the moving median filtering, each burst element is distinguished from the continuum component by the following algorithm. We define a region in the dynamic spectra (hereafter referred to as a window) that has a width of $2t_b$ in time and $2f_b$ in frequency. The radio flux at the center of the window (time $=$ t and frequency $=$ f) is defined as a burst peak flux if it is the maximum flux in the window ($t \pm t_b$ and $f \pm f_b$). The peak fluxes are derived by sliding this window in 10 ms time steps and 61 kHz frequency steps. We used mainly a window that has a time width ($2t_b$) of 100 ms and a frequency width ($2f_b$) of 1.25 MHz (hereafter referred to as a narrower window) because the typical duration and bandwidth of the observed burst elements were several hundred milliseconds and several megahertz, respectively. If several peak fluxes are derived in neighboring bins, the total flux of the bins that are within 200 ms in time and 2.44 MHz in frequency (20 $\times$ 40 bins) of the peak flux bin is derived for every neighboring peak flux bin. Then only one peak flux bin that has the largest total flux is defined as a peak flux to avoid multiple counts for one burst.

The flux at a given time and frequency is defined as a background continuum flux if it is the minimum flux in a time region between $t \pm t_c$. The background continuum fluxes are derived by sliding the $2t_c$ window in 10 ms steps in time and 61 kHz steps in frequency. The time window $2t_c$ is set to 400 ms. The temporal variation in the background continuum component is given by a straight-line approximation of two neighboring continuum fluxes. The radio flux of the burst component is derived by subtracting the background continuum component from the observed radio flux at a given time and frequency.

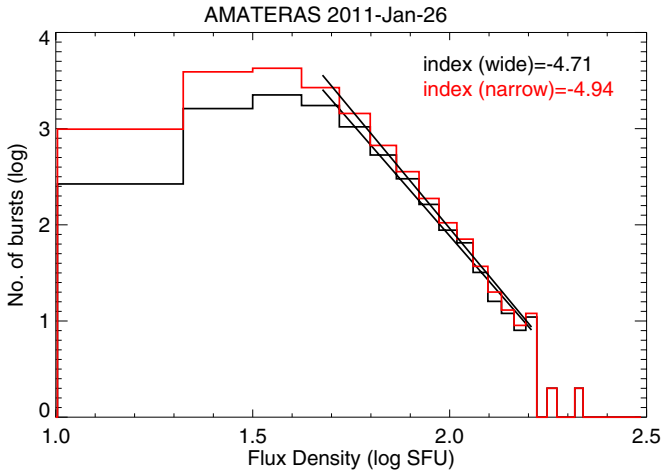

Figure 3. Peak flux distributions of RCP component of type-I bursts observed between 3:00 and 4:00 UT at frequencies of 185.5–197.6 MHz. The horizontal axis indicates the log intensity, and the vertical axis indicates the log number of bursts.

In Figure 2(d), the diamond indicates a burst peak, triangles indicate background continuum, and the rectangle indicates the approximate background continuum flux at the peak time of the burst component. In Figure 2(b), the peak flux of each burst element is shown as a black diamond in the frequency range between 174.5 MHz and 197.6 MHz. This figure shows that each element has single peak flux as shown in one diamond.

Figure 3 shows the peak flux distributions of the RCP component of type-I bursts observed between 3:00 and 4:00 UT at frequencies of 185.5–197.6 MHz. We detected type-I bursts using windows of several sizes and obtained the peak flux distributions. The red line shows the peak flux distribution of

type-I bursts derived with the narrower window, which is a power-law distribution. The spectral index of this power law is about 4.9. The black line shows a peak flux distribution derived with a wider window that has a width of 200 ms in time and 2.44 MHz in frequency. Although the result is similar to that of the narrower window, the number of bursts is smaller in the entire flux density range, and this trend is more significant at weaker flux densities. This is because the large window has missed counts for especially weaker bursts that have shorter durations and narrower bandwidths. This result suggests that detection of radio bursts depends on the window size and that the narrower window is tuned for better detection of both weak and strong bursts.

4. SUMMARY AND DISCUSSION

We observed the fine spectral structures of type-I bursts using the radio telescope AMATERAS. The fundamental spectral structures of type-I bursts are resolved by the high-resolution data from this system. RFI is removed from the observed radio spectra by applying the moving median filter along the frequency axis. We found that data with high frequency resolution are effective for filtering out narrow and fixed-frequency signals using the moving median filter. A two-dimensional auto burst detection algorithm was developed to distinguish each type-I burst element from complex noise storm spectra. The analysis result shows that each type-I burst element has one peak flux without multiple counts or missed counts. The peak flux distribution of type-I bursts derived using this algorithm follows a power law with a spectral index between 4 and 5.

This study deals with a burst element that is on the order of 100 ms in duration and several megahertz in bandwidth because the observed burst elements have a duration and bandwidth on the order of 100 ms and several megahertz. These burst parameters are consistent with previous observations (e.g., Kattenberg & van der Burg 1982) despite the use of our higher-resolution data. There might be some smaller spectral structures that are not resolved by our observational specifications. However, the individual burst element has a smooth light curve (see Figure 2(d)). This suggests that even if there are smaller spectral structures in the radio source region, they have lost their original structure during propagation because of, for example, coronal scattering. Therefore, we conclude that the fundamental burst element can be resolved in our observations.

The peak flux distribution of type-I bursts followed a power law with a spectral index between 4 and 5. The observed spectral index is larger than that of previous studies (Mercier & Trottet 1997; Ramesh et al. 2013). This may be attributed to the difference in the resolutions of the radio spectra because measurements without appropriate time or frequency resolution may cause unrealistic peak flux distribution (Isliker & Benz 2001). This study used observations with high temporal and frequency resolution in a wide observation band. Hence, burst elements are resolved in both time and frequency. We also analyzed the radio dynamic spectra two-dimensionally, in contrast to previous studies that derived the peak flux at fixed frequencies. This difference in analysis methods may also produce different results. Differences in tuning the time and frequency scales for the burst detection can also modify the derived peak flux distributions (see the red and black lines in Figure 3). This study has solved these problems by using highly resolved radio spectra and a new burst detection algorithm which is tuned for better detection of both weak and strong bursts. Therefore, it is not surprising that we found such a soft distribution of type-I bursts for the first time.

There are several candidates to explain the power-law distribution. SOC (Bak et al. 1987) is known to produce a power-law peak flux distribution such as the avalanche model (Rosner & Vaiana 1978; Aschwanden et al. 1998; Aschwanden 2011). These models have usually been used to explain flares that have spectral index smaller than 2. The cascading of a MHD disturbance can form power-law distribution. This model was used to explain the power-law distribution of radio spike bursts in some works (e.g., Karlicky et al. 1996). The spectral index of this model, however, should be 5/3 because of the Kolmogorov's law, so that there are no models that can explain such a soft spectral index observed in this study.

The major problem is that a radio burst is the final result and contains much information. Solar radio bursts occur as a consequence of many plasma processes such as particle acceleration, wave generation, and radio emission and propagation. All these processes could affect the characteristics of the observed radio bursts. Distinguishing the effects of these processes is still difficult, even though we have used high-resolution observational results from AMATERAS. This study has established a method of analyzing complex metric radio spectra. In addition to our analysis, it may be necessary to combine imaging observations and numerical simulation in further studies to identify the generation mechanism of type-I bursts.

AMATERAS is a Japanese radio telescope developed and operated by Tohoku University. This work was conducted under the joint research program of the Solar-Terrestrial Environment Laboratory, Nagoya University.

REFERENCES

Akabane, K. 1956, PASJ, 8, 173
Aschwanden, M. J. 2011, SoPh, 274, 119
Aschwanden, M. J., Dennis, B. R., & Benz, A. O. 1998, ApJ, 497, 972
Aurass, H., Boehme, A., & Karlicky, M. 1990, SoPh, 130, 19
Aurass, H., Hofmann, A., Magun, A., Soru-Escaut, I., & Zlobec, P. 1993, SoPh, 145, 151
Bak, P., Tang, C., & Wiesenfeld, K. 1987, PhRvL, 59, 381
Benz, A. O., & Wentzel, D. 1981, A&A, 94, 100
Cairns, I. H., & Robinson, P. A. 1998, ApJ, 509, 471
Chertok, I. M., Kahler, S., Aurass, H., & Gnezdilov, A. A. 2001, SoPh, 202, 337
Eastwood, J. P., Wheatland, M. S., Hudson, H. S., et al. 2010, ApJL, 708, L95
Elgarøy, Ø. 1977, Solar Noise Storms (New York: Pergamon)
Hannah, I. G., Hudson, H. S., Battaglia, M., et al. 2011, SSRv, 159, 263
Isliker, H., & Benz, A. O. 2001, A&A, 375, 1040
Iwai, K., Miyoshi, Y., Masuda, S., et al. 2012a, ApJ, 744, 167
Iwai, K., Tsuchiya, F., Morioka, A., & Misawa, H. 2012b, SoPh, 227, 447
Karlicky, M., Sobotka, M., & Jiricka, K. 1996, SoPh, 168, 375
Kattenberg, A., & van der Burg, G. 1982, SoPh, 77, 231
Kontogeorgos, A., Tsitsipis, P., Caroubalos, C., et al. 2006, ExA, 21, 41
Mercier, C., & Trottet, G. 1997, ApJL, 474, L65
Meszarosova, H., Karlicky, M., Veronig, A., Zlobec, P., & Messerotti, M. 2000, A&A, 360, 1126
Morioka, A., Miyoshi, Y., Masuda, S., Tsuchiya, F., Misawa, H., Matsumoto, H., Hashimoto, K., & Oya, H. 2007, ApJ, 657, 567
Nita, G. M., Fleishman, G. D., & Gary, D. E. 2008, ApJ, 689, 545
Ramesh, R., Raja, S., & Narayanan, S. 2013, ApJ, 762, 89
Robinson, P. A., Smith, H. B., & Winglee, R. M. 1996, PhRvL, 76, 3558
Rosner, R., & Vaiana, G. S. 1978, ApJ, 222, 1104
Rozhansky, I. V., Fleishman, G. D., & Huang, G.-L. 2008, ApJ, 681, 1688
Shimizu, T. 1995, PASJ, 47, 251
Spicer, D. S., Benz, A. O., & Huba, J. D. 1982, A&A, 105, 221